

Influence of bubbles and sand on chlorophyll-*a* fluorescence measurements in the surfzone

Melissa M. Omand,* Falk Feddersen, David B. Clark, Peter J.S. Franks, James J. Leichter, and R.T. Guza
Scripps Institution of Oceanography, San Diego, CA, USA

Abstract

Continuous chlorophyll-*a* (Chl*a*) measurements in the surfzone (region of wave-breaking adjacent to the shoreline) would increase understanding of harmful algal blooms, food supply for intertidal invertebrates and fishes, and the fate of terrestrial runoff pollution. Optical measurements of Chl*a* fluorescence in the surfzone are affected by bubbles and suspended sand. Here, errors in surfzone Chl*a* fluorescence measurements (using WET Labs ECO Triplet fluorometers) are estimated by comparing observed (Chl*a*_{raw}) with known (Chl*a*_{true}) Chl*a* concentrations in laboratory tests with controlled amounts of bubbles and suspended sand (characterized with concurrently measured optical turbidity, τ). For both bubbles and sand, Chl*a*_{raw} and τ are linearly correlated, and the regression line slope depends on Chl*a*_{true}. When Chl*a*_{true} is low, Chl*a*_{raw} is biased high, and when Chl*a*_{true} is high, Chl*a*_{raw} is biased low. Fluorometers were also deployed in a natural surfzone, and for the limited range of field Chl*a* observed, the field and laboratory τ -Chl*a* relationships were largely consistent. Mechanisms responsible for these biases are proposed, and correction procedures using the observed τ -Chl*a* relationship are developed and applied to surfzone Chl*a*_{raw} observations. For the moderate Chl*a*_{true} concentrations (2–4 $\mu\text{g L}^{-1}$) encountered, errors in hourly mean and instantaneous Chl*a*_{raw} are less than 5% and 15%, respectively. Larger errors are expected for Chl*a*_{true} outside this range. Although further testing is needed, the results suggest that in situ, optical Chl*a*_{raw} from other turbid environments (e.g., estuaries, bays) should also be interpreted cautiously.

Introduction

Chlorophyll-*a* fluorescence (Chl*a*), often used as a proxy for phytoplankton biomass (e.g., Falkowski and Kiefer 1985), is measured by laboratory extraction from discrete water samples (Chl*a*_{true}) or continuously with in situ optical fluorometers (Chl*a*_{raw}). The fast sampling and convenience of in situ optical instruments are advantageous, and in situ Chl*a* sampling is common in the open ocean and on continental shelves. Light scattering near the ocean surface is generated by a variety of

seawater constituents, including bubbles, sand, plankton, and detritus (e.g., Stramski et al. 2004). The relative contributions of these constituents to the total light scattering are variable over time and space. For example, beneath open-ocean breaking waves, bubble-induced light scattering spans several orders of magnitude over time periods of minutes (Terrill et al. 2001). Optical Chl*a* measurements are affected by scattering from particulates, and so data from very near the surface and seafloor (where the concentration of scatterers is highest) are often discarded.

Continuous Chl*a* measurements in the surfzone (region of wave-breaking adjacent to the shoreline) could aid understanding of harmful algal blooms, food supply for intertidal invertebrates and fishes, and the fate of terrestrial runoff pollution. Because of wave breaking and strong currents in shallow water (few meters depth), sediment suspended from the sea bottom, and bubbles injected at the surface, can intermittently populate the entire water column (e.g., Deane and Stokes 1999). The relative contributions of sand and bubbles to a point measurement of surfzone light scatter is not understood, but backscatter is known to depend on cross-shore location and distance above the seafloor (Wang et al. 2002). Backscattered light is known to be problematic for accurate measurement of fluorescent dye with benchtop fluorometers

*Corresponding author: E-mail: momand@ucsd.edu

Acknowledgments

B. Woodward, B. Boyd, K. Smith, D. Darnell, I. Nagy, M. McKenna, and M. Rippy assisted in testing the fluorometers and collecting field observations. SIO Hydro Lab staff and WET Labs personnel provided advice during laboratory tests, and an anonymous reviewer provided very helpful comments on the manuscript. This research was supported in part by California Sea Grant, NOAA, California Coastal Conservancy, and Office of Naval Research. Sea Grant support was through the California Sea Grant College Program Project R/CZ-196, through NOAA's National Sea Grant College Program, U.S. Department of Commerce. The statements, findings, conclusions, and recommendations are those of the authors and do not necessarily reflect the views of California Sea Grant or the U.S. Department of Commerce.

(Smart and Laidlaw 1977) and in situ in the surfzone (Clark et al. 2009). In this article, we characterized the fluorometer response in turbid water and developed methods to correct continuously observed $Chl a$ in the surfzone and (potentially) other turbid environments.

Turbidity from a calibrated nephelometer (τ , nephelometric turbidity units or ntu) characterizes the water cloudiness by observing the amount of emitted light that is backscattered by particles, relative to a secondary standard of clear water. Turbidity depends on the particle concentration, size, shape, and internal index of refraction, as well as the emitted light wavelength and details of the optics (e.g., Zaneveld et al. 1979). The single-frequency turbidity sensors used here provide a bulk estimate of the scattering by all particles in the sample volume.

The influence of bubbles and sand on $Chl a_{raw}$ is explored by simultaneously measuring $Chl a_{raw}$ and τ with a WET Labs ECO Triplet fluorometer. Two τ -related mechanisms can distort ECO Triplet $Chl a_{raw}$ (Fig. 1). Sand and bubbles can scatter light emitted from the τ channel into the $Chl a$ detector. The wavelength ranges of the τ emitter and $Chl a$ detector overlap (personal communication, WET Labs personnel, technical specifications unavailable), elevating (e.g., enhancing) $Chl a_{raw}$ (mechanism A, Fig. 1A). This mechanism is explored by observing $Chl a_{raw}$ with and without the τ emitter blocked. Sand and bubbles also scatter and absorb excited and fluoresced light away from the $Chl a$ emitter/detector, thereby reducing $Chl a_{raw}$ (mechanism B, Fig. 1B). This mechanism is evaluated over a range of bubble- and sand-induced τ for a range of known $Chl a_{true}$ concentrations. Fluorometers were also deployed in a natural surfzone, and field and laboratory τ - $Chl a$ relationships were consistent within the limited range of field $Chl a$ observed. Correction procedures using the observed τ - $Chl a$ relationship were developed and applied to surfzone $Chl a_{raw}$ observations. The effect of fluorescent dye (mechanism C, Fig. 1C) and sunlight (mechanism D, Fig. 1D) on $Chl a_{raw}$ and the τ response of a flow-through WET Labs WETStar fluorometer are discussed in the appendix.

Materials and procedures

ECO Triplet fluorometer—Laboratory and field tests used four 3-channel WET Labs ECO Triplet Fluorometers (www.wet-labs.com) that measure $Chl a$ (470/695 nm excitation/emission wavelengths, 0–150 $\mu\text{g L}^{-1}$ range), Rhodamine-WT dye (540/570 nm excitation/emission wavelengths, 0.2–500 ppb range), and backscattered turbidity (660 nm wavelength, 0.03–100 ntu range). In the field, ECO Triplets internally stored the 3.8-s average of 8-Hz samples. In the lab, 8-Hz samples were averaged for about 1 s. Before testing, the ECO Triplets were calibrated with natural phytoplankton populations (collected from the SIO pier) to within 4% of the WET Labs–provided $Chl a$ calibration. The WET Labs–provided calibration for turbidity was used to convert the backscatter from counts to units of ntu.

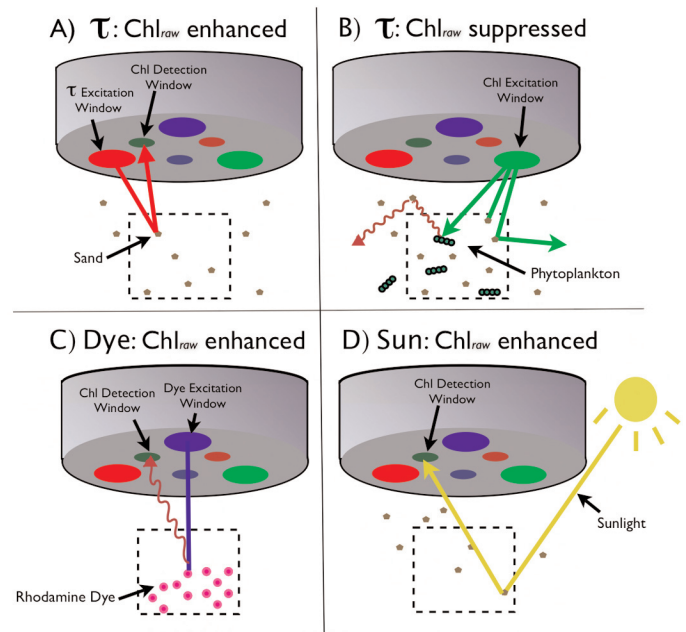


Fig. 1. Schematic of the three-channel ($Chl a$, turbidity, dye) WET Labs ECO Triplet and four potential mechanisms for $Chl a$ error. The dashed box represents the sample volume, located a few centimeters from the 10-cm-diameter sensor head. (A) $Chl a_{raw}$ enhancement through scattering of the 660-nm turbidity excitation into the $Chl a$ detection window (mechanism A). (B) $Chl a_{raw}$ suppression through scattering of the fluoresced 685-nm light away from the $Chl a$ detection window (mechanism B). (C) $Chl a_{raw}$ enhancement through detection of dye fluorescence as $Chl a$ (mechanism C). (D) $Chl a_{raw}$ enhancement through ambient sunlight near 685 nm scattered into the $Chl a$ detection window (mechanism D). The $Chl a$ detection window wavelength range overlaps with the range of emitted τ (A) and dye-fluoresced light (D).

Laboratory methods—To reduce the effect of ambient light, laboratory tests were performed in a round 15-L (30 cm diameter) black-lined bucket with a downward pointing ECO Triplet. In fresh, $Chl a$ -free water, boundary effects (significant and slight enhancement in τ and $Chl a_{raw}$, respectively) were evident only within 5 cm of the bucket wall or bottom. Elsewhere τ and $Chl a_{raw}$ were near zero, indicating minimal interference from bucket wall reflections where the tests below were performed.

The effect of bubble-generated τ on $Chl a_{raw}$ was measured by injecting, into water with known $Chl a_{true}$, controlled quantities of bubbles using a balsa wood bubbler attached to the end of an air hose. The hose air pressure was adjusted so that the bubble-induced τ range was similar to surfzone field tests (0–90 ntu). Nominal bubble radius ranged from 1 to 5 mm, representative of surfzone bubbles (Deane and Stokes 1999).

Similar tests were done with controlled amounts of suspended sand. Dry sand from Scripps Beach (mean diameter approximately 0.2 mm) was kept in a dry, dark container for at least 1 week to eliminate fluorescence from live phytoplankton attached to the grains. Sand-induced τ was generated by stirring up to 200 g of dry sand in the 15-L bucket. Laboratory

sand concentrations (0–13 g L⁻¹) were comparable to instantaneous near-bed concentrations observed in sandy beach surfzones (e.g., Yu et al. 1993, Beach and Sternberg 1996), and the turbidity range was similar to field observations (0–90 ntu).

Phytoplankton, obtained by towing 60-µm mesh nets from the SIO pier in La Jolla, CA, were mixed with sand-filtered (Chla ~0.1 µg L⁻¹) seawater to obtain five samples (10 L each) with Chla between 0.2 and 10 µg L⁻¹. Chla_{true} was measured by filtration of a 150-mL water sample onto 25-mm GF/F filters, extraction in 10 mL acetone, and assessment with a calibrated Turner Designs 7000 benchtop fluorometer. Three extractions at each Chla concentration indicate reproducibility to less than 0.5 µg L⁻¹.

Chla_{raw} field measurements—A month-long field experiment was conducted at Huntington Beach, CA, in fall 2006. Seven bottom-mounted instrumented (temperature, pressure, and current) frames were deployed on a 160-m long cross-shore transect (from 0 to 4 m depth, relative to mean sea level), that spanned the surfzone for the wave conditions encountered. Pressure sensor data were used to calculate hourly significant wave height and the tidally varying mean sea surface. Four ECO Triplet fluorometers were repeatedly deployed for 72-h periods on different frames, facing 30 degrees from downward, nominally 50 cm above the seafloor.

Assessment

In undisturbed (no bubbles or sand) freshwater with Chla_{true} = 0, τ and Chla_{raw} were approximately 0 ntu and 0 µg L⁻¹, respectively (Fig. 2, shaded region from 0–50 s). With the addition of bubbles, τ and Chla_{raw} spiked as high as 95 ntu and 7 µg L⁻¹, respectively (Fig. 2, nonshaded regions). When bubbling stopped, τ and Chla_{raw} dropped to near zero (Fig. 2, gray-shaded region near 205 s). Sporadic Chla_{raw} spikes occurred (e.g., Chla_{raw} = 7 µg L⁻¹ at time 190 s, Fig. 2) and were filtered by rejecting data where the Chla_{raw} rate of change exceeded 1 µg L⁻¹ s⁻¹, a threshold selected to remove large spikes while retaining most of the data. This spike filter, applied to all laboratory Chla_{raw} data, removed between 15% and 35% of data points. After spike removal, Chla_{raw} and bubble-induced τ were significantly correlated (slope [α] = 0.008 ± 0.001 µg L⁻¹ ntu⁻¹, r² = 0.41, P < 0.001) (Fig. 3A), indicating that mechanism A (Fig. 1A) enhances the measured Chla_{true}. Similarly, Chla_{raw} and sand-induced τ were correlated (α = 0.0046 ± 0.0005 µg L⁻¹ ntu⁻¹, r² = 0.64, P < 0.001) (Fig. 3C). The τ-induced enhancement was reproduced in all four ECO Triplets tested.

To confirm that light from the τ channel enhances Chla (mechanism A, Fig. 1A), the Chla = 0 tests were repeated with the τ light excitation blocked on one ECO Triplet. A second, adjacent ECO Triplet measured τ. After spike-filtering, τ excitation-blocked Chla_{raw} was near zero and uncorrelated with τ for both sand and bubbles (Fig. 3B,D), confirming that for these Chla_{true} = 0 tests, the dominant noise source is enhancement from the τ channel.

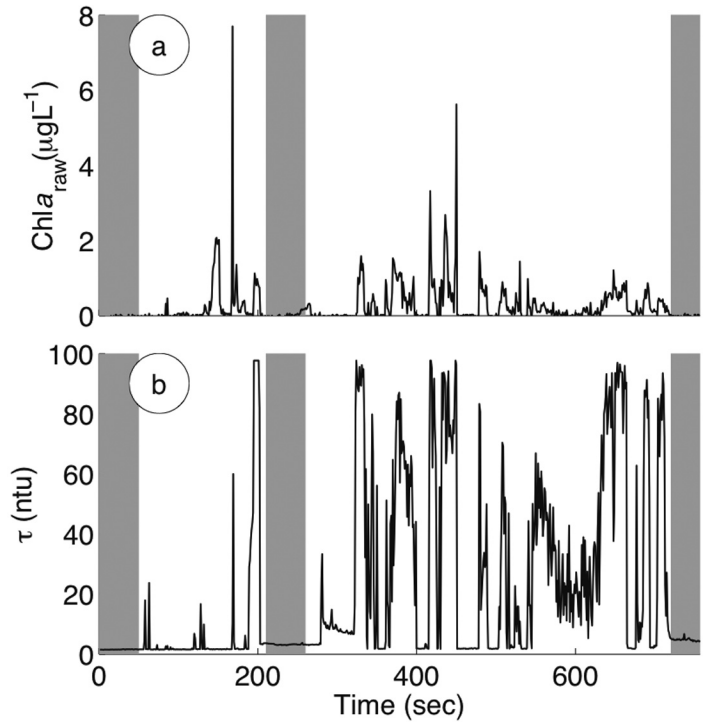


Fig. 2. Measured Chla_{raw} (A) and bubble-induced turbidity τ (B) versus time in fresh, Chla-free water with no ambient light. Vertical gray bars indicate times without bubbles.

In seawater with Chla_{true} = 10 µg L⁻¹ (typical of a coastal phytoplankton bloom), the τ-Chla_{raw} relationship is opposite that for Chla_{true} = 0 µg L⁻¹ (Fig. 4). In undisturbed seawater, τ remained steady at 5 ntu (shaded regions in Fig. 4). When bubbles were added, Chla_{raw} and τ were inversely related (unshaded regions in Fig. 4), with Chla_{raw} decreasing by 40% at high τ, indicating that mechanism B (Fig. 1B) is dominant. When bubble injection intermittently ceased (gray-shaded regions, Fig. 4), τ and Chla_{raw} returned to undisturbed levels.

The observed τ and Chla_{raw} (at fixed Chla_{true}) are linearly related (Fig. 5) and may be described by the following equation:

$$\text{Chla}_{\text{raw}}(\tau) = \text{Chla}_{\text{true}} + \gamma\tau. \tag{1}$$

Nonlinear (quadratic and exponential) fits were also explored, but did not improve the goodness of fit (e.g., Akaike and Bayesian Information Criteria [AIC-BIC], Schwarz 1978). For bubble-induced turbidity tests (Fig. 5A), the slope (γ) of the τ-Chla_{raw} fit depends on Chla_{true}, ranging from enhancement at 0.2 µg L⁻¹ (mechanism A) to strong suppression at 10 µg L⁻¹ (mechanism B). Near Chla_{true} = 4 µg L⁻¹, γ ~ 0 and the two mechanisms approximately cancel. Sand-generated τ and Chla_{raw} show a similar, but less pronounced, pattern (Fig. 5B).

A proposed model for the relationship between Chla_{raw} and τ is

$$\text{Chla}_{\text{raw}}(\tau) = \text{Chla}_{\text{true}} + \alpha_{-} + \beta_{n}(\text{Chla}_{\text{true}})^n\tau, \tag{2}$$

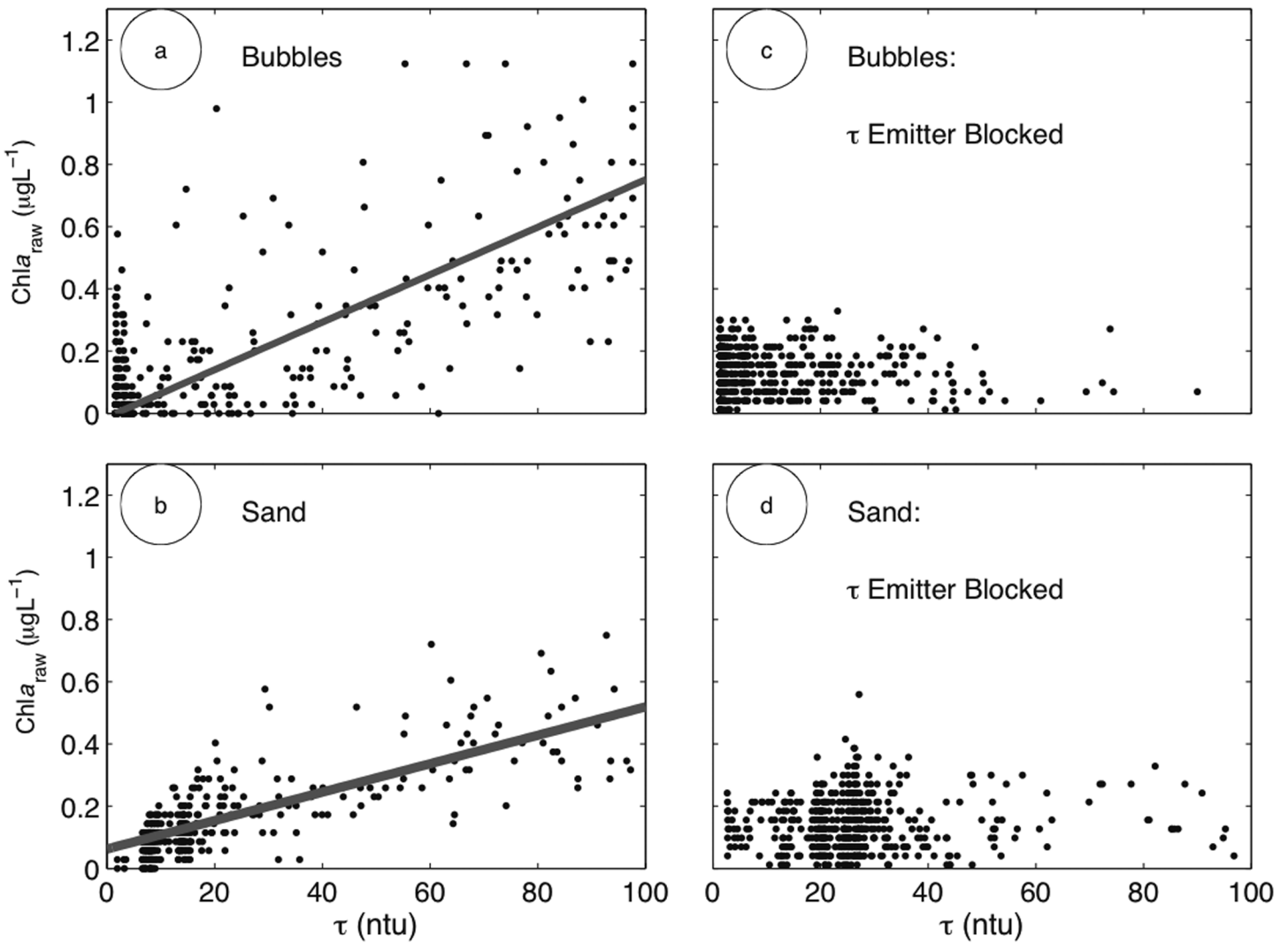


Fig. 3. $Chl a_{raw}$ versus turbidity (τ) (black points) and linear best fit (gray line) in $Chl a$ -free freshwater with no ambient light with bubble-induced τ (slope = $0.008 \pm 0.001 \mu g L^{-1} ntu^{-1}$, $r^2 = 0.41$, $P < 0.001$) (A) and sand (slope = $0.0046 \pm 0.0005 \mu g L^{-1} ntu^{-1}$, $r^2 = 0.64$, $P < 0.001$) (B). $Chl a_{raw}$ with τ emission blocked versus turbidity (black points) in fresh, $Chl a$ -free water with no ambient light, and with bubble-induced ($r^2 = 0.01$, $P = 0.24$) (C) and sand-induced ($r^2 = 0.002$, $P = 0.63$) (D) turbidity.

where the second and third terms on the righthand side represent mechanisms A and B, respectively, α and β are empirically determined constants, and the exponent n is an integer. Using Eq. 2, the dependence of the slope γ (Eq. 1) on $Chl a_{true}$ is

$$\gamma = \alpha + \beta_n (Chl a_{true})^n. \tag{3}$$

In agreement with Eq. 3, γ observed depends nearly monotonically on $Chl a_{true}$, and model fits with $n = 1$ and $n = 2$ were explored (solid and dashed curves in Fig. 6). For the bubbles tests, the quadratic fit ($n = 2$) improved the AIC-BIC over the linear fit ($n = 1$); however, both are encompassed with the error bars on γ at $Chl a_{true} < 10 \mu g L^{-1}$. For the sand tests, the linear fit was most appropriate (black line in Fig. 6). Choice of an optimal model (linear or quadratic) likely will depend on the observed $Chl a_{true}$ range. For small ranges in $Chl a_{true}$, the

quadratic approaches the linear model, whereas for a large range in $Chl a_{true}$, the relationship will be strongly dependent on the choice of n . Bubble-generated turbidity yields $\beta_2 \sim 0.001 \mu g L^{-1} ntu^{-1}$ for the quadratic fit, and $\beta_1 \sim 0.01 ntu^{-1}$ (nearly 10 times larger than the $\beta_1 \sim 0.001 ntu^{-1}$ for sand). For single-channel fluorometers (no τ channel), suppression (mechanism B) is present. Tests with a single channel WETStar fluorometer and a separate τ sensor in a flow-through package agree qualitatively with Eq. 2 with $\alpha = 0$ (Appendix 1C).

The laboratory tests were conducted with either bubbles or sand only. In the surfzone, bubbles and sand are both present, in unknown amounts, so the appropriate α and β_n for field applications are unknown. The α and β_n obtained from sand-only and bubble-only lab tests are considered an envelope for the range in $Chl a$ error.

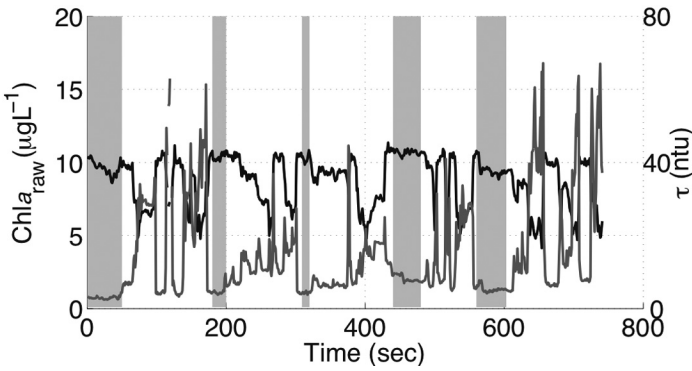


Fig. 4. $Chla_{raw}$ (black) and bubble-induced turbidity (dark gray) versus time in seawater with $Chla_{true} = 10 \mu\text{g L}^{-1}$. Vertical gray bars indicate times without bubbles.

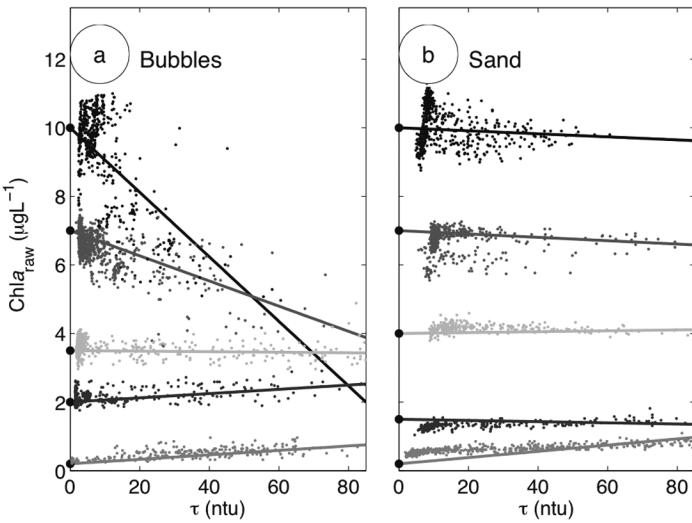


Fig. 5. $Chla_{raw}$ versus turbidity (τ) in seawater with 5 known $Chla_{true}$ concentrations (black asterisks on vertical axis corresponding to 10, 7, 4, 1.5, and 0.2 $\mu\text{g L}^{-1}$) for bubble-induced (A) and sand-induced (B) τ . Solid lines are linear fits with intercept set equal to $Chla_{true}$. The fraction of variance described by each fit (in ascending $Chla_{true}$ order) is $r^2 = 0.48, 0.45, 0.05, 0.22, 0.52$ (bubbles) and $r^2 = 0.10, 0.01, 0.01, 0.46, 0.70$ (sand). The r^2 in bold type correspond to $P < 0.001$.

Discussion

Surfzone field observations are examined in light of laboratory tests showing that turbidity generates $Chla_{raw}$ errors that depend upon $Chla_{true}$. Field data were retained only if the ECO Triplet was more than 1 m below the mean free surface, thus reducing the effect of scattered sunlight (Appendix 1C) and excluding observations (usually at low tide) when the sensor pierced the water surface in wave troughs. The spike filter (a cutoff of 0.25 $\mu\text{g L}^{-1} \text{ s}^{-1}$ was chosen for field data because the ECO Triplets were sampled at 0.25 Hz rather than the 1-Hz lab sample rate) removed obvious $Chla_{raw}$ spikes while preserving 95% of the data.

Laboratory tests examined τ -induced errors in $Chla_{raw}$ with known, fixed $Chla_{true}$ (Figs. 4, 5, and 6). Field data segments

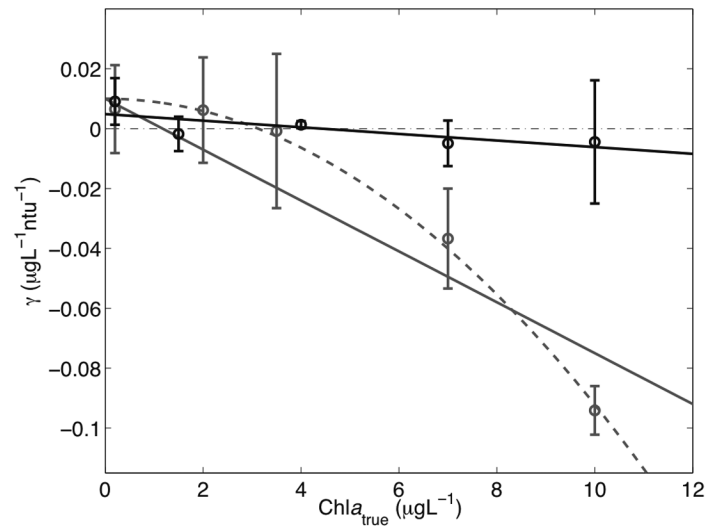


Fig. 6. Laboratory τ - $Chla_{raw}$ regression slopes γ (from Fig. 5) versus $Chla_{true}$ for bubble (gray) and sand (black) tests. The solid lines are linear regression fits (Eq. 3) with intercepts ($\alpha = 0.008 \pm 0.001 \mu\text{g L}^{-1} \text{ ntu}^{-1}$ [bubbles] and $\alpha = 0.0046 \pm 0.0005 \mu\text{g L}^{-1} \text{ ntu}^{-1}$ [sand]) determined from $Chla_{true} = 0$ tests. The linear best-fit slopes β_1 are $-0.010 \pm 0.003 \text{ ntu}^{-1}$, $r^2 = 0.90$, $P = 0.01$ (bubbles) and $-0.0011 \pm 0.0003 \text{ ntu}^{-1}$, $r^2 = 0.59$, $P = 0.12$ (sand). The gray dashed line represents the best quadratic fit for bubbles ($\beta_2 = -0.001 \mu\text{g L}^{-1} \text{ ntu}^{-1}$) with intercept ($\alpha = 0.008 \pm 0.001 \mu\text{g L}^{-1} \text{ ntu}^{-1}$) determined from $Chla_{true} = 0$ tests. The black dot-dashed line at $\gamma = 0$ indicates the border between τ -induced enhancement ($\gamma > 0$) and suppression ($\gamma < 0$).

are selected for comparable analysis. $Chla_{nat}$ for each 3-h segment is defined as the $Chla_{raw}$ values when $\tau < 10 \text{ ntu}$ (gray points, Fig. 7). Of 250 original segments, 85 were retained with (1) small $Chla_{nat}$ variation (standard deviation $< 1 \mu\text{g L}^{-1}$) and (2) broad variation in τ (upper τ limit $> 50 \text{ ntu}$). For the 85 cases, $Chla_{raw}$ was typically low ($< 5 \mu\text{g L}^{-1}$), and $Chla_{raw}$ and τ were often significantly correlated (r^2 ranging between 0.2 and 0.6). Linear best fits between $Chla_{raw}$ and τ yield γ values for each 3-h segment (Fig. 7) that are similar to laboratory γ with known, fixed $Chla_{true}$ (Fig. 5). Extracted $Chla$ from bottle samples were not available for each of these time periods and fluorometer locations, thus the median $Chla_{nat}$ ($Chla_{m-nat}$) was assumed to approximate $Chla_{true}$. The field γ - $Chla_{m-nat}$ relationship (where τ is caused by a mix of bubbles and sand) is bounded by the results from lab tests with sand and bubbles introduced separately (shaded region, Fig. 8). The field $Chla_{m-nat}$ range is limited between 1 and 4 $\mu\text{g L}^{-1}$. Within this range, a quadratic relationship between γ and $Chla_{m-nat}$ did not improve the fit (according to the AIC-BIC). Therefore, for the observed $Chla_{m-nat}$ range, a linear model ($n = 1$) was considered most appropriate. For larger $Chla_{true}$, this may not be appropriate. The γ - $Chla_{m-nat}$ relationship may differ within and seaward of the surfzone owing to the different contributions of breaking wave-induced bubbles and sand to turbidity. However, the fit skill and intercept within and seaward of the surfzone are not statistically different, so an α_{field} and β_{field}

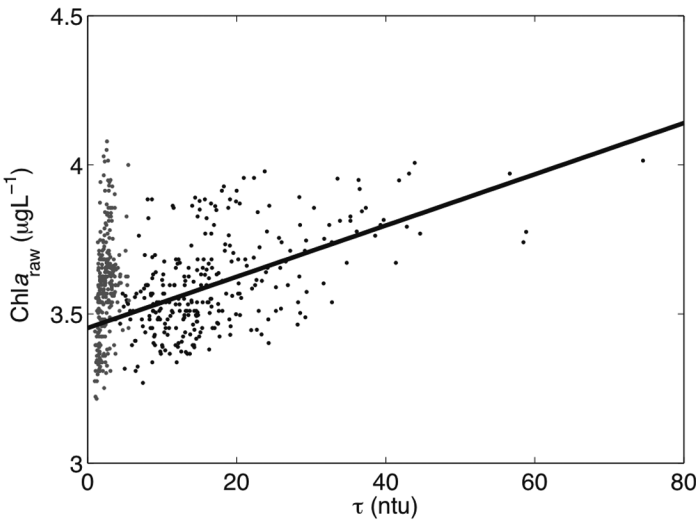


Fig. 7. $Chla_{raw}$ versus turbidity (τ) within the surfzone for a single 3-h period. Each dot is a 4-s observation. The gray points ($Chla_{nat}$) are $Chla_{raw}$ with $\tau < 10$ ntu, and the median $Chla_{nat}$ ($Chla_{m-nat}$) approximates $Chla_{true}$ for this period. The black dashed line is a linear best fit (slope [γ] = $0.0086 \mu\text{g L}^{-1} \text{ntu}^{-1}$, $r^2 = 0.29$, $P < 0.001$).

(representing all data) were selected. The model parameters optimizing the linear fit are $\beta_{field} = -0.004 \pm 0.002 \mu\text{g L}^{-1} \text{ntu}^{-1}$ and $\alpha_{field} = 0.017 \mu\text{g L}^{-1}$.

Typical variations of τ , tides, waves, and $Chla$ are illustrated with 48 h of observations at two fixed locations, one within the surfzone, and the other further seaward (Fig. 9). Wave heights at the seaward location varied less than 10% from 0.55 m (Fig. 9C). At lower tide stages, the shallow instrument was near the surface, occasionally exposed in wave troughs, and τ and $Chla_{raw}$ were noisy (Fig. 9A and D). Data from less than 1 m below the surface were discarded, and spikes removed (black line, Fig. 9E). Corrections for the τ -induced errors are based on Eq. 2, with $n = 1$:

$$Chla_{corr}(t) = \frac{Chla_{raw}(t) + \alpha_{field}\tau(t)}{1 + \beta_{field}\tau(t)} \quad (4)$$

where t is time. The corrected (red line, Fig. 9E) and raw (black line, Fig. 9E) data are similar for the range of $Chla_{raw}$ encountered. The instantaneous (and hourly mean) errors induced by τ reach 15% (5%) within the surfzone (black line, Fig. 9F) and are negligible seaward (gray line, Fig. 9F). With the modest range of observed $Chla_{raw}$, the model (Eq. 1) predicts that τ -generated errors in $Chla_{raw}$ seaward of the surfzone would be limited to 1% (at 5 ntu), whereas errors within the surfzone would surpass 15% (above 30 ntu).

Turbidity depended on the cross-shore location (within or seaward of the surfzone) and decreased with depth below the surface. At the most-offshore fluorometer (~160 m from shore), τ was below 5 ntu 90% of the time, and $Chla_{raw}$ typically ranged between 2 and 7 $\mu\text{g L}^{-1}$ (gray lines, Fig. 10). Within the surfzone (~20 m from shore), the τ range was

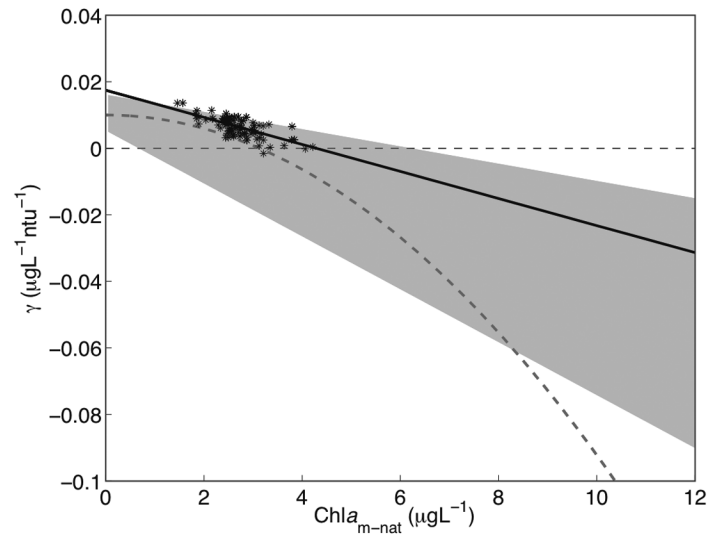


Fig. 8. Field-derived τ - $Chla_{raw}$ regression slopes γ versus $Chla_{m-nat}$ (asterisks). The solid line is the least-squares fit, $r^2 = 0.48$, $P < 0.001$, slope (β_{field}) = $-0.004 \pm 0.002 \mu\text{g L}^{-1} \text{ntu}^{-1}$, intercept (α_{field}) = $0.017 \mu\text{g L}^{-1}$. The gray shaded region indicates the laboratory γ range with linear fits ($n = 1$) to the bubbles and sand tests, and the gray dashed line indicates the quadratic fit to the bubbles laboratory test (see Fig. 6). The black dashed line at $\gamma = 0$ indicates the border where τ -induced enhancement ($\gamma > 0$) and suppression ($\gamma < 0$) are dominant.

larger, falling below 30 ntu 90% of the time, and the $Chla_{raw}$ range was smaller than offshore (black lines, Fig. 10).

Natural $Chla_{true}$ variability may be driven by advection of horizontal and vertical phytoplankton patches, cell growth and death, phytoplankton behavior (swimming or sinking), or physiological adaptations to light. Nearshore $Chla$ levels are often variable. For example, $Chla_{true}$ was $< 1 \mu\text{g L}^{-1}$ 10.0% and $> 10 \mu\text{g L}^{-1}$ 7.4% of the time in biweekly bottle samples from the SIO pier (~5 m total depth; La Jolla, CA, SCCOOS.org) between April 2005 and April 2008. During these time periods, if τ reached 50 ntu, bubble- and sand-induced ECO Triplet errors (assuming a linear [$n = 1$] relationship between γ and $Chla_{true}$) would be on the order of 80% (low $Chla_{true}$) and 20% (high $Chla_{true}$), respectively (Fig. 11a). In single-channel fluorometers when mechanism A is not present, the ratio between $Chla_{raw}$ and $Chla_{true}$ would depend on τ , and under moderate surfzone conditions (30 ntu) and moderate $Chla_{true}$, $Chla_{raw}$ would underestimate $Chla_{true}$ by 15% (Fig. 11B). In some highly productive areas, $Chla_{true}$ frequently surpasses $10 \mu\text{g L}^{-1}$, and during intense blooms, may reach $>100 \mu\text{g L}^{-1}$ (e.g., Kudela and Cochlan 2000). Under these circumstances, a more detailed investigation of the nonlinear relationship between $Chla_{true}$ and γ (see Fig. 6) is required.

Sudden, intense appearances of specific species of phytoplankton are known as harmful algal blooms (HABs) because of toxins (e.g., *Pseudonitzschia* spp., Sayce and Horner 1996), mechanical damage (e.g., *Chaetoceros* spp., Tester and Mahoney 1995) or anoxia (e.g., *Ceratium* spp., Mahoney and

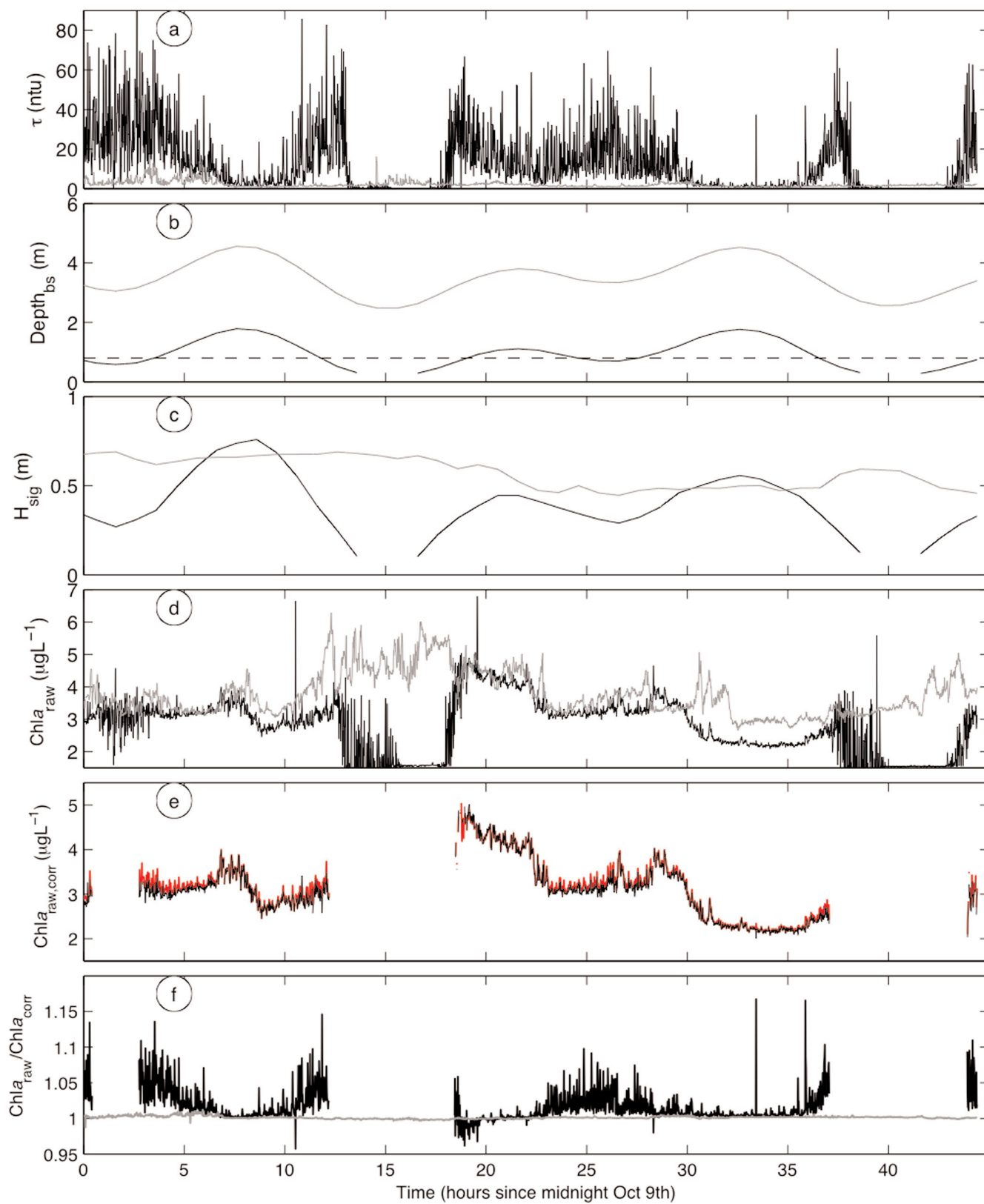


Fig. 9. (A) Turbidity τ . (B) $Depth_{bs}$, distance instrument is below mean sea surface (dashed line is 1 m). (C) Significant wave height H_{sig} . (D) Unprocessed $Chla_{raw}$. (E) Surfzone $Chla_{raw}$ (despiked, observations within 1 m of the surface removed, black) and $Chla_{corr}$ (red). (F) $Chla_{raw}/Chla_{corr}$. All versus time for 48 h. Gray (black) lines correspond to data seaward of (within) the surfzone.

Steml 1979) associated with them. The greatest ecological and economic costs incurred by HABs are observed in nearshore environments where benthic populations and aquaculture are exposed. Satellite-derived Chl*a* estimates are commonly used for HAB monitoring. Pfister et al. (2007) compared Chl*a* data from SEAWIFS satellite measurements and a flow-through WETStar fluorometer moored within a tide pool (1.1 m total depth) at Tatoosh Island, WA. Despite various quality controls, remotely sensed Chl*a* and moored Chl*a* were poorly

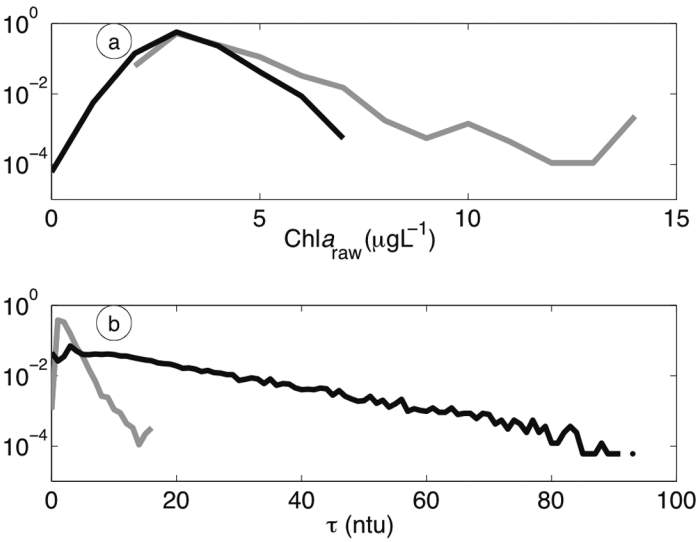


Fig. 10. Probability density function of despiked Chl*a*_{raw} (A) and turbidity (B) for all field data (~500 h) inside (black line) and outside (gray line) the surfzone.

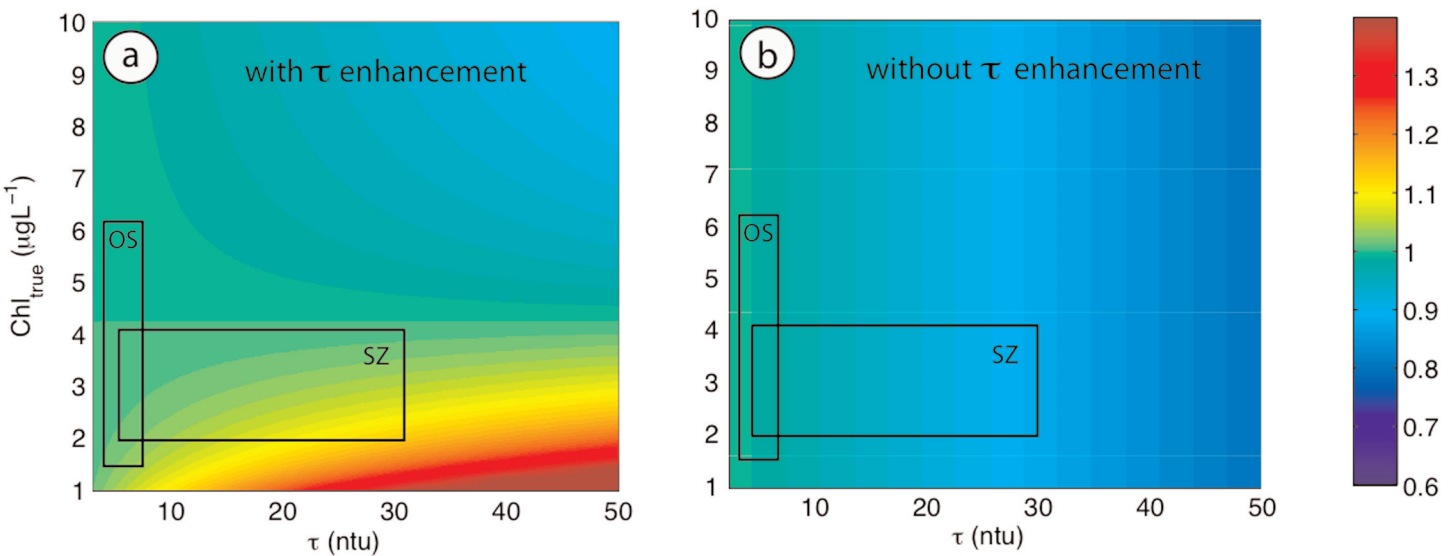


Fig. 11. Predicted Chl*a*_{raw}/Chl*a*_{true} ratio with field-derived parameters ($n = 1$, α_{field} and β_{field}) for ECO Triplet fluorometers over a range of Chl*a*_{true} and τ values with τ enhancement (A) and without τ enhancement (B) due to emitted τ interference ($\pm = 0$). The white boxes represent the ranges of 90% of Chl*a*_{true} and τ measurements taken within the surfzone (SZ) and seaward of the surfzone (OS) during the field experiment.

correlated. Pfister et al. (2007) suggested a variety of explanations that may have contributed to the poor correlation. An additional explanation for the poor correlation may be the turbidity-induced error in this shallow nearshore environment (see Appendix 1C for bubble-induced Chl*a*_{raw} error with a WETStar fluorometer). This poor correlation emphasizes the importance of extensive comparisons between satellite and in situ monitoring stations, and also the necessity for improved understanding of the potential instrument response in these sometimes turbid environments.

Comments and recommendations

The effect of bubble- and sand-generated turbidity on measured Chl*a* fluorescence has been estimated for WET Labs ECO Triplet fluorometers using both laboratory tests and field observations. The results are summarized as follows: (1) Sporadic spikes in Chl*a*_{raw} (in lab and field) are common under turbid conditions and can be removed. (2) For low Chl*a*_{true} concentrations (<4 µg L⁻¹), turbidity enhances the Chl*a*_{raw} signal by scattering a fraction of the emitted τ light into the Chl*a* detector (mechanism A, Fig. 1A). For Chl*a*_{true} > 4 µg L⁻¹, turbidity reduces Chl*a*_{raw} relative to Chl*a*_{true} by scattering or absorbing emitted and fluoresced light before detection (mechanism B, Fig. 1B). Laboratory tests indicate that the presence of bubbles or sand (after despiking) induces a false Chl*a*_{raw} signal of up to 1 µg L⁻¹ in Chl*a*-free water, and Chl*a*_{raw} suppression of up to 40% (in water with nonzero Chl*a*) at typical surfzone turbidity levels. (3) In general, Chl*a*_{raw} is more affected by bubble-generated turbidity than by sand-generated turbidity for both mechanism A and mechanism B, but particularly at high Chl*a*_{true} when mechanism B dominates. (4) A linear ($n = 1$) model for the τ -Chl*a*_{raw} slope (γ) best rep-

resents the limited range of $\text{Chl}a_{\text{raw}}$ observed in the field. The dependence of γ on $\text{Chl}a_{\text{true}}$ ($\sim\text{Chl}a_{\text{m-nat}}$) is consistent between lab and field observations, suggesting that the laboratory tests were representative of field surfzone conditions. Although a quadratic ($n = 2$) model best described the laboratory tests with bubble-induced turbidity, a linear model was the most appropriate for our limited field data set. (5) This $\tau\text{-Chl}a_{\text{raw}}$ model can be used to approximately correct data and to estimate error bounds for $\text{Chl}a_{\text{true}}$ less than $10 \mu\text{g L}^{-1}$. Observations over a greater range of $\text{Chl}a_{\text{true}}$ are required before extrapolating the linear model for γ to correct high $\text{Chl}a_{\text{raw}}$ concentrations. (6) Rhodamine-WT dye generates a strong false Chl*a* signal and therefore precludes reliable coincident measurements of Chl*a* (mechanism C, Fig. 1C; Appendix 1A). (7) Incident irradiance may enhance $\text{Chl}a_{\text{raw}}$ less than 1 m below the surface (mechanism D, Fig. 1D; Appendix 1B). (8). Bubble-induced turbidity generated qualitatively similar suppression (mechanism B) in a single-channel, flow-through Wetstar fluorometer (Appendix 1C), indicating that this effect applies generally to other fluorometers, not just the ECO Triplet. Caution is recommended in interpreting in situ $\text{Chl}a_{\text{raw}}$ data from turbid environments.

References

- Beach, R., and R. Sternberg. 1996. Suspended-sediment transport in the surf zone: response to breaking waves. *Continent. Shelf Res.* 16:1989–2003.
- Clark, D. B., F. Feddersen, M. M. Omand, and R. T. Guza. 2009. Measuring fluorescent dye in the bubbly and sediment laden surfzone. *Water Air Soil Pollut.*, in press.
- Deane, G. B., and M. D. Stokes. 1999. Air entrainment processes and bubble size distributions in the surf zone. *J. Phys. Oceanogr.* 29:1393–1403.
- Falkowski, P., and D. A. Kiefer. 1985. Chlorophyll-*a* fluorescence in phytoplankton: relationship to photosynthesis and biomass. *J. Plankton Res.* 7:715–731.
- Falkowski, P., and J. A. Raven. 1997. *Aquatic Photosynthesis*. New York: Blackwell Science.
- Kudela, R. M., and W. P. Cochlan. 2000. Nitrogen and carbon uptake kinetics and the influence of irradiance for a red tide bloom off southern California. *Aquat. Microb. Ecol.* 21:31–47.
- Mahoney, J., and E. W. Steiml Jr. 1979. A mass mortality of marine animals associated with a bloom of *Ceratium tripos* in the New York Bight. In *Toxic Dinoflagellate Blooms: Proceedings of the 2nd International Conference*. London: Elsevier, p. 225–230.
- Muller, P., Li, X., and K. K. Niyogi. 2001. Non-photochemical quenching: a response to excess light energy. *Plant Physiol.* 125:1558–1566.
- Pfister, C. F., J. T. Wootton, and C. J. Neufeld. 2007. Relative roles of coastal and oceanic processes in determining physical and chemical characteristics of an intensely sampled nearshore system. *Limnol. Oceanogr.* 52:1767–1775.
- Sayce, K., and R. A. Horner. 1996. Pseudo-nitzschia spp. in Willapa Bay, Washington, 1992 and 1993. In *Harmful and Toxic Algal Blooms*. Proc. 7th Int. Conf. Toxic Phytoplankton. Intergov. Oceanogr. Comm. UNESCO, p. 131–134.
- Schwarz, G. 1978. Estimating the dimension of a model. *Ann. Stat.* 6:461–464.
- Smart, P., and I. Laidlaw. 1977. Evaluation of some fluorescent dyes for water tracing. *Water Resource Res.* 13:15–33.
- Stramski, D., E. Boss, D. Bogucki, and K. J. Voss. 2004. The role of seawater constituents in light backscattering in the ocean. *Prog. Oceanogr.* 61:27–56.
- Terrill, E. J., M. Kendall, and D. Stramski. 2001. Bubble entrainment by breaking waves and their influence on optical scattering in the upper ocean. *J. Geophys. Res.* 106:16815–16823.
- Tester, P. A., and B. Mahoney. 1995. Implication of the diatom, *Chaetoceros convolutus*, in the death of red king crabs, *Paralithodes camtschatica*, Captains Bay, Unalaska Island, Alaska. In *Harmful Marine Algal Blooms*. Proc. 6th Int. Conf. on Toxic Marine Phytoplankton. Lavoisier, p. 95–100.
- Wang, P., B. A. Ebersole, E. R. Smith, and B. D. Johnson. 2002. Temporal and spatial variations of surf-zone currents and suspended sediment concentration. *Coast. Eng.* 46:175–211.
- Wilson, J. F., E. D. Cobb, and F. A. Kilpatrick. 1986. Fluorometric procedures for dye tracing. *Applic. Hydraulics* 3:15–33.
- Yu, Y., R. W. Sternberg, and R. A. Beach. 1993. Kinematics of breaking waves and associated suspended sediment in the nearshore zone. *Continent. Shelf Res.* 13:1219–1242.
- Zaneveld, J. R. V., R. V. Spinrad, and R. Bartz. 1979. Optical properties of turbidity standards. *SPIE* 208:159–168.

Submitted 11 March 2008

Revised 3 February 2009

Accepted 22 February 2009